Applied Catalysis A, General 685 (2024) 119873

Contents lists available at ScienceDirect

Applied Catalysis A, General

journal homepage: www.elsevier.com/locate/apcata

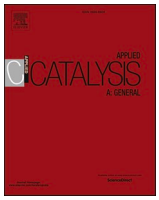

Insights into the development of greener mild zeolite dealumination routes applied to the hydrocracking of waste plastics

Muhammad Usman Azam [a], Waheed Afzal [a,*], Auguste Fernandes [b], Inês Graça [a,*]

[a] School of Engineering, University of Aberdeen, Aberdeen, Scotland AB24 3UE, UK
[b] Centro de Química Estrutural, Institute of Molecular Sciences, Instituto Superior Técnico, Universidade de Lisboa, Av. Rovisco Pais, Lisboa 1049-001, Portugal

ARTICLE INFO

Keywords:
Greener zeolite dealumination
Hierarchical zeolites
Life cycle assessment
HDPE hydrocracking
Catalyst recyclability

ABSTRACT

This study highlights novel, energy-efficient, environmentally friendly and less time-consuming methods to dealuminate zeolites, by forced convective steaming and use of molecular CO_2. Zeolites with comparable (or superior) physicochemical properties than those of traditional dealumination techniques were produced. All dealuminated zeolites were tested for the hydrocracking of high-density polyethylene, showing considerably high activity and selectivity for lighter oils, particularly gasoline. The forced convective steamed zeolite revealed to be the best, given its high number of silanol groups, acidity and porosity, and lower environmental impact. Furthermore, bi-functional Ni-loaded dealuminated zeolites showed good stability and ability to be regenerated. Therefore, it is possible to generate hierarchical zeolites by dealumination with physicochemical and catalytic properties comparable to their rival technologies, following green chemistry metrics. Given the relevance of hierarchical zeolites in sustainable routes to produce chemicals and fuels, the potential of application of these newly developed catalysts is highly promising and vast.

1. Introduction

Zeolites are crystalline aluminosilicates that possess well-defined porous systems of varying sizes and tuneable physicochemical properties [1]. Due to these properties, they have been extensively used in various refining and petrochemical industrial catalytic applications, such as cracking [2,3], alkylation of aromatics [4], reforming [5], dewaxing [6], isomerization of xylenes [7], and during the electrolysis process [8,9]. More recently, attention has been devoted to the generation of zeolites with improved diffusional properties, either by the creation of wider porous structures or by decreasing the diffusional paths. This aids in reducing mass transfer constraints of reactants and products to and from the active centre, particularly when dealing with bulkier molecules. Additionally, it prevents undesired side reactions caused by the microporous channels of zeolite, which can lead to coking, catalyst deactivation and most significantly, the wastage of zeolite materials and energy. As a result, zeolites with such characteristics are quite appealing for many catalytic applications i.e., Friedel−Crafts alkylation of arenes [10], cracking of plastics to liquid fuels [11,12] Fischer−Tropsch synthesis (FTS) process for the production of clean hydrocarbon fuels or chemicals from syngas [13], direct oxidation of benzene to phenol [14] and many others [15,16].

Therefore, ongoing research and development efforts have been focused on improving the accessibility of the active sites within zeolite frameworks via the formation of ultra-larger pores zeolites (ULP), zeolite nanocrystals with shorter diffusion paths and hierarchically modified zeolites with combined micro- and mesopores. However, the poor structural stability, loss of acidity and high synthesis cost of ULP zeolites have limited their practical applicability. Similarly, the synthesis of nanocrystal zeolites also faces many obstacles, since it involves the use of hazardous and costly templates, with serious implications to the environment [2]. On the other hand, hierarchical zeolites incorporate the benefits of multi-level porosity [16] that assist in the mobility of bulky molecules and decrease the probability for the catalyst to deactivate owing to the reduction of molecules retention time within the structure, while presenting comparable crystallinity and functionality than their parent counterparts [17].

The obtention of hierarchical zeolites can be either by bottom-up (soft or hard templating) or top-down methodologies (i.e., desilication or dealumination). Amongst all, the top-down technique based on the dealumination of zeolite is affordable and considered as a promising approach with practical applications [17,18]. It consists of a

* Corresponding authors.
E-mail addresses: waheed@abdn.ac.uk (W. Afzal), i.graca@abdn.ac.uk (I. Graça).

https://doi.org/10.1016/j.apcata.2024.119873
Received 9 May 2024; Received in revised form 24 June 2024; Accepted 5 July 2024
Available online 8 July 2024

post-synthesis procedure, utilizing organic or inorganic acids or through hydrothermal treatment with water vapour (steaming), where mesoporosity is generated by the elimination of aluminium, either framework and/or extra-framework species, from the zeolite [19]. Despite the significant advantages towards the affordability and formation of mesoporosity, removal of framework and/or extra-framework aluminium may be accompanied by a significant loss in the number of Brønsted and Lewis acid sites if dealumination conditions are not tightly controlled, which is not advantageous for some catalytic applications. Moreover, the conventional dealumination methods, i.e., steaming and/or acid leaching, limit the sustainable properties of the resulting dealuminated zeolites, as steaming at high temperatures is generally an energy-intensive and time-consuming process, whereas acid leaching significantly produces aqueous acidic wastes [20]. Thus, it is required to optimize these methods to strike a balance between degree of dealumination and acidity with retained crystallinity, while complying with green chemistry metrics.

Therefore, this research focuses on the development of mildly dealuminated zeolites to be applied to the current problem associated with the management of waste plastics. Conventionally, waste plastics are managed by incineration and/or landfill. However, life cycle assessment of these management scenarios has demonstrated a notable generation of greenhouse gases (GHGs), dioxins, and furans as by products, which limits the sustainable nature of these technologies. In addition, plastics, being derived from petroleum, are difficult to recycle due to their bulky and complex chain molecular structure. However, over the last few years, advanced methods based on feedstock and/or chemical recycling of waste plastics have emerged, which aim at transforming non-recycled plastics into alternative fuels, high value-added chemicals or raw materials for use in new manufacturing processes. It encompasses a variety of procedures which can include photo reforming [21], depolymerization [22], deconstruction [23], gasification [24], thermal [25], and catalytic pyrolysis [25,26], or hydrocracking of waste plastics [27,28]. Amongst all, hydrocracking offers many benefits when compared to alternative thermal and catalytic methods. This exothermic process not only enables lower reaction temperatures, thereby decreasing the energy required for the process, but also results in high selectivity for more stable valuable products (i.e., paraffins). It also enables a circular economy by utilizing plastics as a feedstock to produce fuels that mitigate the requirement for ongoing feedstock procurement and could transform significant economic losses into benefits. Hydrocracking over a bifunctional Ni-loaded mildly dealuminated zeolite under a reductive atmosphere revealed to be appealing, since the improved porosity and external surface area enable the diffusion of bulky polymeric chains into the zeolite framework, where strong acid sites crack the carbon–carbon bonds together with the hydrogenation of intermediates over Ni species and prevent catalytic coking [29].

Herein, faujasite (FAU) type Y zeolite is utilized as a benchmark catalyst because of its industrial application in petroleum refineries for fluid catalytic cracking (FCC) and hydrocracking [30]. Similarly, in comparison to other 3-dimensional zeolites, including HZSM-5 and β-zeolite, Y zeolite exhibits better textural properties (i.e., pore volume and surface area), which is critically important for the diffusion of bulkier polymeric molecules into the channels of the zeolite [29,31] whereas the mild acidity helps to control the cracking extent and reduce coke deposition [32]. Therefore, the optimum balance between acidity and textural properties of Y zeolite is indeed required to produce lighter oils with relatively high selectivity of gasoline range hydrocarbons, making it a suitable candidate for the hydrocracking of plastics. Moreover, a high silica zeolite (Si/Al= 30) was chosen to precisely monitor the effect of degree of dealumination of the various routes, since it is more difficult to dealuminate a Y zeolite with a high Si/Al ratio in comparison to lower Si/Al ratios. A similar work has been recently carried out by Zhou et al. [33] who studied the dealumination of Y zeolite with relatively higher Si/Al ratio (17.5). This also allows to directly compare the hydrocracking results of the present study with the available literature where researchers have mainly used Y zeolites with Si/Al ratios of 30–50 [29,34,35]. Two greener routes by forced convective steaming and molecular CO_2 treatment for the dealumination of this HY zeolite were carried out and compared to conventional dealumination procedures via steaming and acid leaching. A mild dealumination was performed to avoid significant reduction of the acidic properties of the zeolites and not to compromise their crystalline structure. The physiochemical properties of all the prepared dealuminated materials were compared to those of the parent HY zeolite. Moreover, the benefits of the proposed routes (i.e., forced convective steaming and molecular CO_2 treatment) for the dealumination of HY zeolites, when compared with the traditional steaming and acid leaching methods, were analysed by life cycle assessment (LCA) and utility costing. The state-of-the-art developed catalysts with and without the addition of metal (i.e., Ni) were tested for the hydrocracking of virgin high density polyethylene (HDPE). The performances of the modified Ni-loaded dealuminated Y zeolites were also compared and evaluated in terms of product distribution for the hydrocracking of HDPE. The stability and reusability of various Ni-loaded dealuminated HY zeolites for the hydrocracking of post-consumed HDPE were investigated and compared. Overall, this work discusses the balance and importance of the catalytic properties of the produced materials (controlled dealumination, porosity, acidity and concentration of silanol groups) for the hydrocracking of HDPE.

2. Experimental

The information related to chemicals and materials utilized, detailed experimental and characterization procedures and life cycle assessment is part of the Supporting Information (SI).

2.1. Preparation of dealuminated Y zeolites

Starting with the commercial Y zeolite (Si/Al = 30), dealuminated HY zeolite samples were prepared according to the procedures explained below. Fig. 1 highlights the schematic diagrams of various techniques used to prepare the dealuminated HY zeolite samples.

Conventional Dealumination Techniques:

- Steaming: the commercial HY zeolite was thermally treated at 500 °C for 4 h under a 100 mL.min^{-1}.g^{-1} continuous flow of air saturated with water at room temperature (i.e., 2.3 kPa, saturation pressure of water at 20 ℃ as calculated by Antoine equation). The prepared sample is steamed dealuminated HY zeolite and denoted as DAHY-S.
- Acid leaching: 1 g of the commercial HY zeolite was added to 33 mL of a diluted aqueous solution of HCl (0.5 mol/L) and stirred for 1 h at 60 ℃. After 1 h, the sample was quickly cooled down to room temperature, filtered and washed several times with deionised (DI) water until neutral pH was achieved, which was followed by drying in an oven at 100 °C overnight. The dried sample was then calcined in a tubular furnace at 500 °C for 6 h under dry air flow of 60 mL.min^{-1}.g^{-1}. The as-prepared dealuminated HY sample was denoted as DAHY-HCl.

New Proposed Dealumination Techniques:

- Forced convective steaming: a known amount of the commercial HY zeolite was added to a crucible and placed in a heater equipped with a convective fan which generated saturated hot air under operation. The bottom side of the heater was charged with DI water (20 mL.g^{-1} of catalyst) and the vessel was operated at 200 °C for only 1 h. The generation of steam (i.e., $P_{sat.}$ = 1552.4 kPa as calculated by Antoine equation) at the high flow of air resulted in the controlled dealumination of zeolite. The resultant sample is denoted as DAHY-CS.
- CO_2 atmosphere: 100 mL.min^{-1} of CO_2 was absorbed in 33 mL of DI water for 15 min followed by the addition of 1 g of commercial HY. The sample was then stirred for 1 h at room temperature over a continuous flow of CO_2 absorbed in DI water in a closed vessel. After

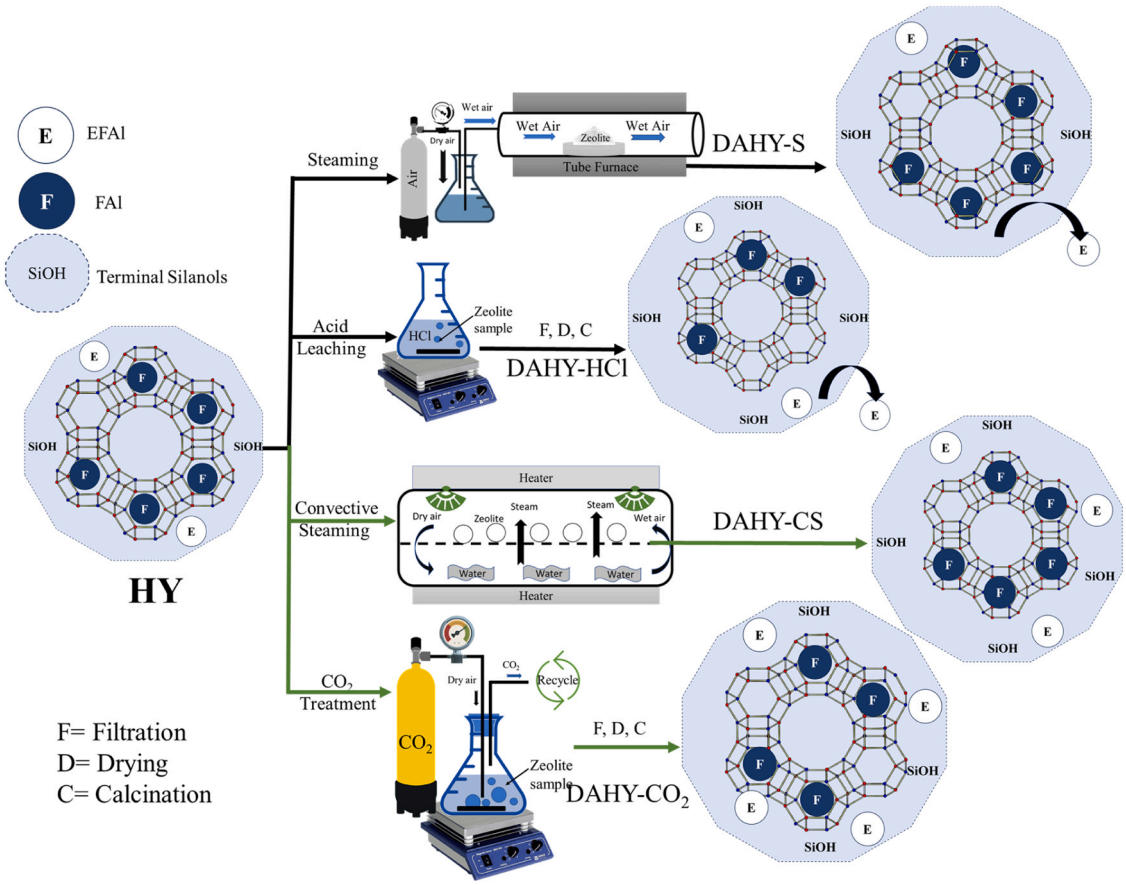

Fig. 1. Schematic diagram for the dealumination of HY zeolite using different approaches.

1 h, the sample was filtered, dried in an oven at 100 °C for 12 h and calcined at 500 °C for 6 h under dry air flow of 60 mL.min^{-1}.g^{-1}. The as-synthesized dealuminated HY zeolite was represented as DAHY-CO_2.

2.2. Preparation of Ni-impregnated Y Zeolite Samples

The Ni-impregnated zeolite samples were prepared by incipient wetness impregnation, using an aqueous solution of $Ni(NO_3)_2.6\ H_2O$ for a final Ni loading of around 5 wt%, as already optimized in our previous work [2]. A calculated volume of an aqueous solution of the metal precursor was added dropwise to the dried HY zeolite support. The Ni-impregnated zeolite samples were calcined at 500 °C for 6 h under dry air flow of 60 mL.min^{-1}.g^{-1} after being dried at 100 °C for 12 h in an oven. The Ni-loaded samples were denoted as Ni-HY (5 % Ni-impregnated commercial HY zeolite), Ni-DAHY-S (5 % Ni-impregnated dealuminated Y zeolite through steaming), Ni-DAHY-HCl (5 % Ni-impregnated dealuminated Y zeolite through acid leaching), Ni-DAHY-CS (5 % Ni impregnated dealuminated Y zeolite through forced convective steaming) and Ni-DAHY-CO_2 (5 % Ni impregnated dealuminated Y zeolite through CO_2 atmospheric treatment).

3. Results and discussion

3.1. Impact of greener dealumination routes

Catalytic hydrocracking of plastics has already been extensively studied in the last two decades, exhibiting significant environmental advantages when compared to pyrolysis and other linear end-of-line waste management options [36,37]. However, none of the previous studies considered the impact associated with the synthesis and/or modification of catalysts. In fact, despite the improved textural and catalytic properties of hierarchical zeolites modified using strong acids, structure directing agent, and/or various template materials, the impact associated with the synthesis procedures may detract the sustainability of the overall process.

Therefore, this research focused on the development of various novel, more energy-efficient, timesaving and environmentally friendly approaches to produce dealuminated zeolites under mild treatment conditions. Greener zeolite dealumination routes such as forced convective steaming and CO_2 treatment were compared with the conventional routes using steam and acid leaching. Table 1 shows the physicochemical properties of the parent and dealuminated zeolites. Analysis of the textural properties of the samples (i.e., porosity and external surface area) reveals that forced convective steaming and molecular CO_2 treatment were as effective as the conventional steaming and acid leaching procedures in increasing the mesoporous volume and external surface area when compared with the parent HY zeolite, while all preserved the microporous volume. In addition, the dealuminated zeolites produced by the greener treatments present number and strength of Brønsted acid sites that are within the same range of those obtained via the conventional routes. On the other hand, an enhancement of the Lewis acidity was observed for the forced convective steaming and molecular CO_2 treatments. The catalytic performance of these zeolites was analysed for the hydrocracking of waste plastics. The forced convective steaming demonstrated higher catalytic activity (60.5 %) in comparison to the conventional steaming (50.1 %). Similarly, molecular CO_2 treated zeolite exhibited similar catalytic activity (52.8 %) as the acid leaching catalysts (54.3 %). Therefore, it can be concluded that it is possible to produce materials by dealumination via the reported greener alternative routes, with comparable or superior

Table 1
Physicochemical properties of the HY zeolite and its various modified samples employed during the hydrocracking of HDPE.

Catalyst Name	Relative intensity	a_o(Å)	Ni[a]	Si/Al[b]	Si/Al_{IV}[c]	FAl[d]	EFAl[d]	ΔSi-OH[e]	Δ-OH[f]	PyH^+	PyL	$\frac{PyH^+_{350°C}}{PyH^+_{150°C}}$	$\frac{PyL_{350°C}}{PyL_{150°C}}$	V_{micro}[g]	V_{meso}[g]	S_{ext}[g]	S_{BET}
	(%)		(wt%)					(cm^{-2})		(μmol.g^{-1})		(%)	(%)	($cm^3.g^{-1}$)		($m^2.g^{-1}$)	
HY	100	24.243	-	30	31	5.95	0.15	-	-	231	42	53	88	0.239	0.248	256	692
DAHY-S	93	24.246	-	29	29	6.34	0.07	4	1.9	237	36	47	89	0.272	0.283	297	784
DAHY-CO_2	90	24.240	-	28	33	5.69	0.93	6.1	-1.5	174	75	45	46	0.230	0.260	283	722
DAHY-CS	92	24.242	-	29	32	5.88	0.52	7.4	2.6	269	57	44	69	0.245	0.264	287	727
DAHY-HCl	87	24.232	-	37	39	4.76	0.29	7.1	-3.5	148	42	28	73	0.239	0.282	301	740
Ni-HY	96	-	5.1	-	-	-	-	-0.16	-2.1	123	269	37	34	0.227	0.224	241	680
Ni-DAHY-S	84	-	4.5	-	-	-	-	3.7	-3.0	96	210	36	39	0.252	0.268	297	760
Ni-DAHY-CO_2	82	-	4.4	-				5.8	-2.2	133	178	36	29	0.237	0.260	281	715
Ni-DAHY-CS	83	-	4.7	-	-	-	-	6.8	-2.5	114	250	34	36	0.240	0.261	286	720
Ni-DAHY-HCl	72	-	4.2	-	-	-	-	6.9	-2.1	136	115	35	37	0.238	0.277	297	727

V_{micro} micropore volume; V_{meso} mesopore volume; S_{ext} external surface area; FAl framework aluminium; EFAL extra-framework aluminium species.
[a] Ni (wt%) determined from H_2-TPR results by using a calibration factor of 1.362×10^{-7} mmol/mV and H_2 consumed.
[b] Global Si/Al determined from elemental analysis (ICP-OES).
[c] Framework Si/Al calculated from the unit cell parameter using the Breck-Flanigen equation. [39]
[d] Calculated based on unit cell parameters.
[e] Difference in the integrated silanol peak area of each sample and the area of the HY zeolite (29.4 cm^{-2}).
[f] Difference in the integrated -OH peak area of each sample and the area of the HY zeolite (7.8 cm^{-2}).
[g] As measured by N_2 physisorption experiments.

physicochemical properties and catalytic performance than the conventional steaming and acid leaching dealumination modifications. Moreover, this has been achieved in a shorter time (1 h for convective steaming), with lower energy requirements (30 times less electricity) and without the production of acidic aqueous waste streams, as generated during the preparation of DAHY-HCl .

To corroborate the higher sustainability of the novel dealumination procedures presented in this work, the environmental profiles of the different modification methods for the dealuminated HY zeolite samples were studied, using a simple life cycle assessment only addressing the modification procedures as per ISO standards and systems. However, the present study excludes the impact associated with the synthesis of commercial zeolites, as the emissions are not directly owned by the entity (i.e., Scope 2 or 3 emissions). Also, it is important to highlight that the present LCA is of a generic nature, aimed at addressing broader objectives. The overall life cycle impact assessment (LCIA) midpoint characterization results for the different HY zeolite modification methods, in terms of global warming potential (kg of CO_2 eq.) and freshwater aquatic ecotoxicity (FWAE, kg 1,4-DB eq.) using the CML-IA baseline method, are illustrated in Fig. 2. Overall, DAHY-CS showed the least impact on climate (0.09 kg CO_2 eq./g) because of the least utilization of electricity, whereas DAHY-HCl showed maximum impact on environment (3.48 kg CO_2 eq./g), which is obvious due to the high energy utilization, as shown in Table S1. For DAHY-S and DAHY-CO_2, impacts of 0.79 and 2.66 kg CO_2 eq./g were respectively observed. One should also consider lowering the global warming impact of the DAHY-CO_2 zeolite by using CO_2 from flue gas (i.e., waste CO_2) and by recovering 100 % CO_2 gas at the end, which would diminish the need for washing, making the process circular and more sustainable. As electricity utilization is the main reason for such global warming potential caused by the various dealuminated HY zeolites, a cost analysis was done after considering a price for electricity of 6.56 cent/kWh [38]. As expected, dealumination using HCl is the costliest technique (0.88 USD/g) closely followed by DAHY-CO_2 (0.86 USD/g), whereas DAHY-CS is the cheapest method (0.03 USD/g).

A similar trend was seen for FWAE, where both DAHY-S and DAHY-CS showed lower impact (i.e., 0.03–0.05 kg 1,4-DB eq.), while DAHY-HCl revealed a 75-fold higher impact (1.89 kg 1,4-DB eq.) due to maximum utilization of resources (i.e., electricity, water, and HCl). On the other hand, modification through molecular CO_2 is responsible for creating an impact of 1.47 kg 1,4-DB eq./g. Similarly, in terms of cost of DI water ($ 0.0282/L), the water costs to modify the HY zeolite through acid leaching is 1.5 cents/g of catalyst (14.5 USD/kg), which is 26-times higher than the price for convective steaming (0.56 USD/kg).

These results highlight the importance of selecting and developing catalysts that align with sustainability principles to minimize environmental impacts. Therefore, the potential of forced convective steaming and effective utilization of CO_2 for the dealumination of zeolite provides an opportunity to develop innovative technologies for producing hierarchical zeolites that are highly energy-efficient with the least environmental impacts and significant relevance on an industrial scale. A detailed analysis of the zeolites' physicochemical properties and catalytic performance are evaluated in the next sections.

3.2. Catalyst characterization

3.2.1. XRD analysis and relative crystallinity of various zeolites

Fig. 3a shows the PXRD patterns for the pristine and modified HY zeolite samples with and without incorporation of Ni. All samples exhibit diffraction peaks at 2θ of 6.2, 10.3, 12.1, 15.9, 18.9, 20.7, 24 and 27.5°, which correspond to the faujasite (FAU) zeolite structure. The Ni-loaded zeolites exhibit a pattern similar to that of the parent HY zeolite, indicating that the zeolite structure remained unchanged during the impregnation process (Fig. 3b). However, the reduced Ni-loaded zeolites did not exhibit any diffraction peaks for Ni species, likely because of the low amount of Ni and/or due to a good dispersion of the metallic Ni

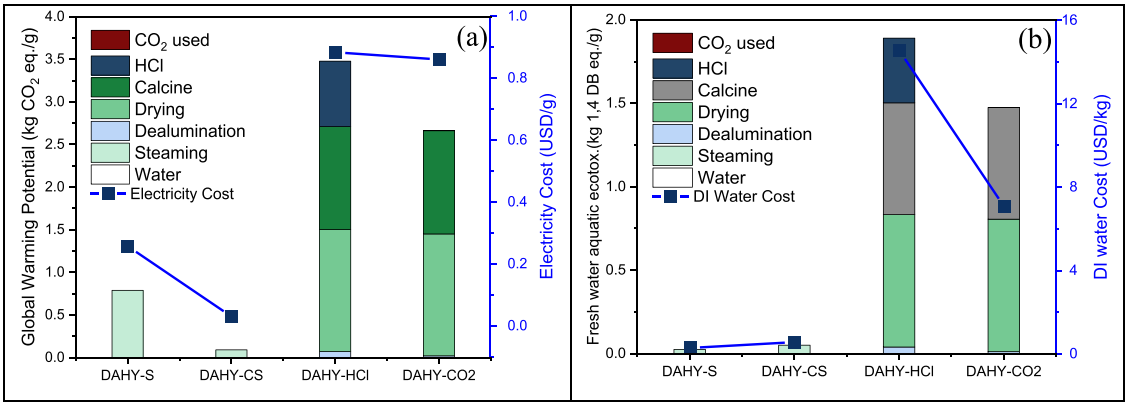

Fig. 2. Impact assessment and utility cost of different modification methods used for dealuminated HY zeolites on (a) global warming potential (kg CO_2 eq.) and (b) freshwater aquatic ecotoxicity (kg 1,4- DB eq.).

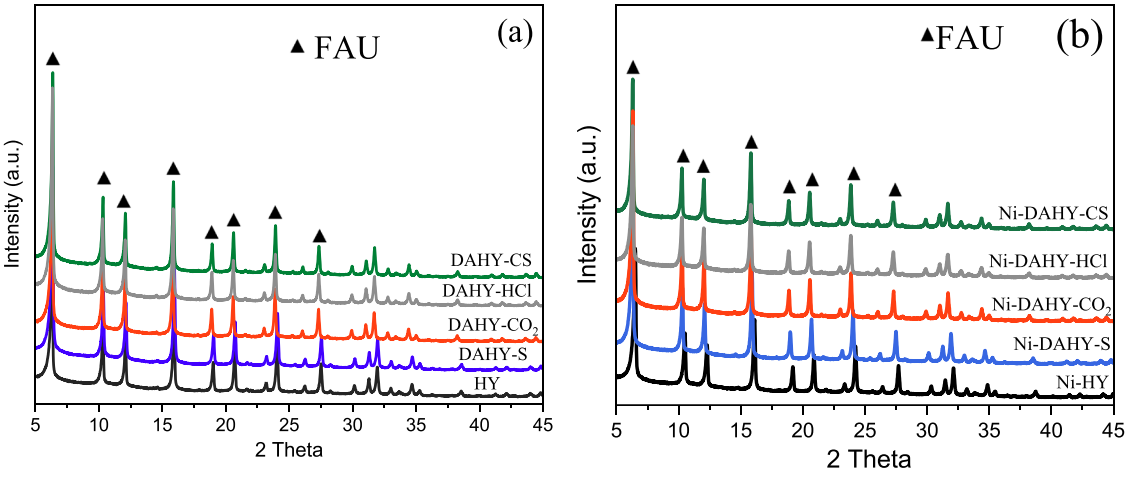

Fig. 3. XRD diffractograms of the (a) parent and dealuminated HY zeolites after calcination and (b) Ni-loaded zeolites after reduction.

particles. Moreover, Table 1 presents the relative crystallinities of all modified samples and that of the parent HY zeolite. Based on the results, there is only a slight decrease in the relative crystallinity of the zeolite after dealumination due to the removal of framework aluminium (FAl) and/or extra-framework aluminium (EFAl) species, indicating that the different modifications did not cause significant damage to the zeolite framework. However, DAHY-HCl showed the lowest relative crystallinity, which may be due to the more severe nature of this treatment. Similarly, the addition of Ni to the framework results in a slight loss of intensity, likely because the added Ni also absorbs XRD radiation (Fig. 3b). Despite this, the Ni-modified samples did not display any peaks due to lower impregnation of Ni-loaded zeolite samples.

3.2.2. *Nitrogen physisorption and elemental analysis*

The amount of Al and Si determined by ICP-OES was used to estimate the global Si/Al of the parent and dealuminated HY zeolites and the results are presented in Table 1. All dealuminated HY zeolites, except DAHY-HCl, exhibited nearly identical global Si/Al ratios to that of the parent HY zeolite. This could either be due to (i) a low or non-removal of framework aluminium (FAl) or (ii) the retention inside the zeolite structure of the extracted aluminium as extra-framework aluminium species (EFAl). For DAHY-HCl, a slightly higher global Si/Al ratio was found, which could indicate a certain degree of removal of aluminium from the zeolite, assuming silicon remains the same. Framework Si/Al ratios were, on the other hand, obtained from the XRD data, by calculating the unit cell parameter for all the samples and applying the Breck-Flanigen equation [39]. For the parent HY zeolite and steamed zeolite, framework and global Si/Al are identical, a slightly larger difference being observed for the other dealuminated samples, which may indicate some removal of framework aluminium.

To investigate this, calculations were made to find the framework aluminium and extra-framework aluminium species, after considering no silicon was extracted. Dealuminated HY zeolite through steaming showed a similar amount of FAl with only the removal of EFAL species from the structure, as discussed in a previous paper [2]. On the other hand, for all the other dealumination treatments, a decrease in the framework aluminium was observed, especially for the DAHY-HCl sample. This was also accompanied by an increase in the EFAl species for all these samples, meaning that part of the extracted aluminium remained in the zeolite structure. Even though the DAHY-HCl sample was the one showing the highest FAl extraction, it has a lower EFAl content than the DAHY-CO_2 and DAHY-CS, which can be due to the leaching of the EFAl species to the aqueous medium. All this corroborates the differences observed in the framework and global Si/Al ratios as indicated above.

Moreover, the removal of FAl and/or EFAl through dealumination is known to be responsible for enhancing the textural properties of the zeolites. The nitrogen isotherms of parent, dealuminated and Ni-loaded zeolite samples are illustrated in Fig. S1. As expected, all the zeolite samples exhibited type IV isotherm which indicates the presence of mesopores in the samples [31]. However, the main difference observed in the N_2 isotherms of the various zeolite samples is the quantity of nitrogen adsorbed (cm^3/g), suggesting a difference in the textural properties of the various zeolites. Therefore, to examine the effect of

dealumination, Table 1 displays the comparison of the textural properties, namely external surface area, BET surface area and pore volumes, of the parent and modified zeolite samples.

Despite the already significant porosity (i.e., both micro- and mesoporosity) of the parent HY, all the dealumination treatments led to an increase in the mesoporosity and external surface area, while preserving the microporous volume. The BET surface area was also observed to increase as a result of the dealumination treatments. Compared to the parent HY zeolite, the steamed and HCl modified samples showed the highest increase in these parameters. For the steamed zeolite, only EFAl were removed as previously mentioned, which opened the pores without creation of additional deposits. In the case of the HCl sample, despite the high FAl extraction, this was accompanied by a higher degree of leaching of the removed aluminium, which helped to additionally increase the porosity. However, the retention of some EFAl species may have led to a smaller increase in the BET surface area as compared to DAHY-S. For the other two zeolites (convective and molecular CO_2), the increases in mesoporous volume and external surface area were not so accentuated because of the removal of FAl and their consequent retention within the structure as EFAl species. This was also accompanied by a lower increase in the BET surface area as compared to DAHY-S and DAHY-HCl. Moreover, the addition of Ni to the HY zeolite resulted in a reduction in the pore volume and external surface area. In contrast, the impregnation of the same quantity of Ni to the dealuminated HY zeolite samples resulted in a decrease in the microporous and mesoporous volumes, whereas the impact on the external surface area was minimal. This suggests that the Ni particles are uniformly loaded and mainly situated inside the zeolite structure in the case of dealuminated HY zeolite samples, as later confirmed by H_2-TPR. In line with this, all samples showed a reduction in the BET surface area after Ni impregnation.

3.2.3. *Analysis of acid sites in various zeolite samples by infrared spectroscopy*

The FTIR spectra before and after pyridine adsorption in the OH-region (3800–3400 cm^{-1}) for the various HY zeolites and their respective Ni-impregnated samples are shown in Fig. 4a and b. The displayed spectra are all identical, with some variations in the intensities of the three primary bands. The bands observed at 3565 and 3630 cm^{-1} are assigned to the Brønsted acid sites, resulting from the vibration of the Al-OH-Si bridging hydroxyl groups in the supercages and sodalite cages, respectively [2]. Table 1 illustrates the difference in hydroxyl groups of the different samples as compared to the parent HY zeolite. Compared with the parent HY zeolite, both steamed and convective steamed HY zeolites showed an increase in the intensities of these OH bands resulting from the vibration of bridging hydroxyl groups, whereas both HCl-leached and molecular CO_2 treated samples showed a decrease. This will be explained later when discussing the Brønsted acidity. The other quite prominent peak at 3740 cm^{-1} is attributed to the existence of weak or non-acidic terminal silanol groups (Si-OH) on the external surface of the zeolite [2]. Interestingly, the parent HY zeolite already shows a noticeable band corresponding to these terminal silanol groups with an integrated area of 29.4 cm^{-1}, which may be associated with the substantial presence of porosity in the material (Table 1). However, all the dealuminated HY zeolite samples exhibit higher band intensity at 3740 cm^{-1}, which shows an increase in the number of terminal silanol groups (Si-OH) as compared to the pristine material. This is not strange considering that dealumination treatments normally result in an increased number of terminal silanol groups, as when material is removed from the zeolite framework, termination units, which are usually Si-OH groups, are required to complete the zeolite chains (Table 1). Moreover, no peaks corresponding to the generation of EFAl species were seen for all the dealuminated HY zeolite samples, although there is an additional generation of EFAl for some of these samples as observed in Table 1. This is because of the following reasons: (i) relatively low amount of EFAl that is not enough to generate a visible band and/or (ii) the overlapping of bands which makes it complicated to observe it. Furthermore, in general all the Ni-impregnated samples showed a decrease in the Brønsted acidic sites (i.e., Al-OH-Si groups) in both the supercages and sodalite cages (Fig. 4b and Table 1). This reduction in Al-OH-Si groups may have been brought on by the insertion of some Ni^{2+} in exchange positions, which is in accordance with the literature [40] and it will be later observed in the DRS UV–vis data. The terminal silanol groups, however, remained almost unchanged by the Ni addition (Table 1). After pyridine adsorption (dotted lines), the bands at 3560 and 3630 cm^{-1} disappear as expected due to their acidic nature, which confirms the accessibility of the pyridine to the bridging hydroxyl groups (Brønsted acid sites) of the zeolites. On the other hand, the addition of pyridine only results in a slight decrease in the silanol band intensity (3740 cm^{-1}), due to the low or non-acidic nature of these OH-groups. The slight decrease may be typically attributed to interactions between Si-OH groups and probe molecules adsorbed on nearby acid sites [41].

Moreover, the difference spectra of pyridine adsorbed at 150 °C for the various HY zeolites and their respective Ni-loaded samples in the range of 1650–1400 cm^{-1} are shown in Fig. S2a and b. The bands at 1455 and 1623 cm^{-1} belong to coordinatively adsorbed pyridine in the "classical" Lewis acid sites corresponding to EFAL species (LAS, PyL),

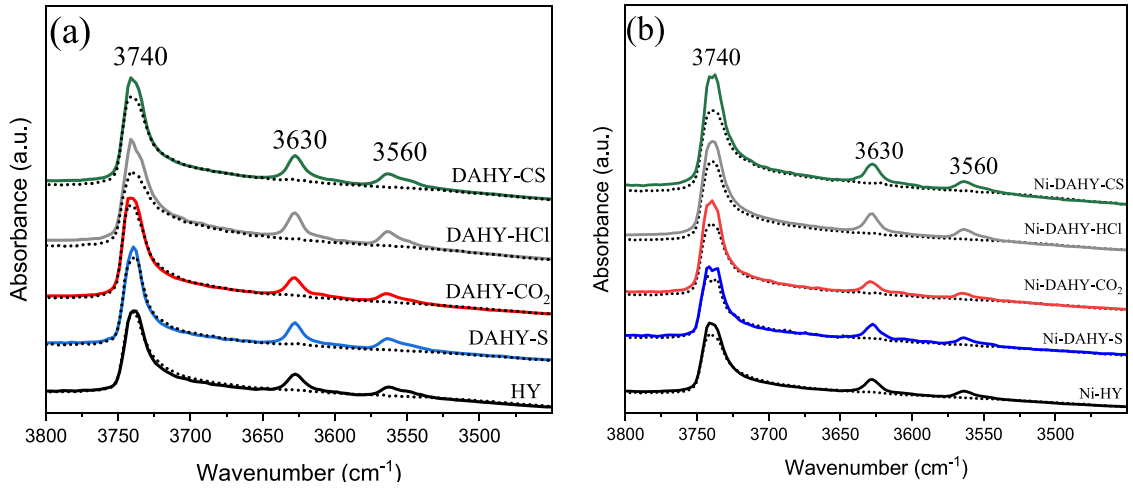

Fig. 4. FTIR spectra in the OH-region (3800–3400 cm^{-1}) before (continuous line) and after (dotted lines) pyridine adsorption for the (a) parent and dealuminated HY zeolite samples, and (b) Ni-loaded zeolite samples.

while the bands at 1547 and 1640 cm^{-1} are attributed to the pyridinium ions interaction with Brønsted acid sites (BAS, PyH^+). The sharp band observed at 1490 cm^{-1} is associated with the interaction of pyridine with both BAS and LAS. However, the addition of Ni results in the appearance of two stronger bands at 1610 and 1450 cm^{-1}, attributed to the coordination of pyridine to divalent Ni^{2+} cations [42–44]. Similarly, another small band at 1575 cm^{-1} appeared which might be either due to the interaction with Ni species and/or attributed to co-ordinately bonded pyridine at LAS [44]. However, this band is more intense in Ni-impregnated zeolite samples.

Table 1 summarises the acidic properties (i.e., the concentration of Brønsted and Lewis acid sites and their strength) of the parent HY and the various dealuminated HY zeolite samples, with and without the addition of Ni. Interestingly, the various mildly dealuminated Y zeolites with different degrees of dealumination showed different concentrations of BAS and LAS. Overall, both DAHY-S and DAHY-CS showed a small increase in the concentration of BAS, whereas DAHY-CO_2 and DAHY-HCl exhibited a decrease in concentration of BAS, as in agreement with the changes observed for the bridging hydroxyl vibrations bands. For the DAHY-S, the slight increase in the number of Brønsted acid sites is not surprising taking into account that no framework aluminium was removed and the accessibility to the pores may have increased owing to the removal of some EFAl species. This is consistent with the textural properties of the DAHY-S which showed the highest increase in the microporous volume as compared to the other samples (Table 1). On the other hand, for the DAHY-CS, this positive impact of the treatment on the BAS is an unexpected outcome, considering that a certain degree of FAl extraction took place (Table 1). However, this removal was not as high as for DAHY-CO_2 and DAHY-HCl zeolites and this sample showed the second highest increase in the microporous volume. Therefore, an increase in pores accessibility may have played a more significant role. Finally, both DAHY-CO_2 and DAHY-HCl zeolites led to a decrease in the concentration of BAS due to the notable removal of FAl species. On the other hand, DAHY-S led to a slight decrease in the concentration of LAS, whereas all the other samples showed an increase in the number of LAS. This agrees with the removal of only EFAl species for the steamed zeolite, while for all the other samples the number of EFAl species increased due to the dealumination treatments. Looking at the results in Table 1, there is indeed a good correlation between the number of EFAl species and the amount of Lewis acid sites. Moreover, the incorporation of Ni over zeolite resulted in a decrease in the concentration of BAS with a significant increase in the LAS [45]. The reduction in BAS could be due to the introduction of Ni^{2+} in exchange positions as compensating cations, which agrees with the observed decrease in the band intensities of Ni-loaded zeolites at 3565 and 3630 cm^{-1} (Fig. 4b). In addition, the incorporation of Ni leads to an increase in the Lewis acid sites, which may be both due to the presence of NiO species and some exchanged Ni^{2+} ions that present Lewis acid character [40,46]. To confirm this, the decrease in Brønsted acid sites (ΔPyH^+) and increase in Lewis acid sites (ΔPyL) for different Ni-loaded zeolite, with respect to their respective parent material, were calculated as a function of Ni-loading (Fig. S2c and d). It is indeed possible to see that the reduction in Brønsted acid sites due to Ni is smaller than the increase in the Lewis acidity showing that both NiO and Ni^{2+}-exchanged species can in fact contribute to the Lewis acid sites.

Furthermore, Table S2 illustrates the evolution of the concentration of BAS and LAS with the increase in the temperature. Overall, the concentration of Brønsted acid sites decreases with the increase in the temperature. Most of the dealuminated zeolites (without Ni) seem to have similar acidity strength at 350 ℃, except for the HCl-treated sample, for which the ratio of BAS at 350 and 150 ℃ is much lower (Table 1). DAHY-HCl showed weak Brønsted acidic strength possibly due to the harsh modification conditions, with removal of stronger BAS, and maximum removal of EFAl as already discussed above. After addition of Ni, an identical decrease in the number of BAS able to retain pyridine at 350 ℃ was observed for all the Ni-containing samples (Table 1, and S2), as the introduction of Ni is not expected to significantly change the acidity strength of the catalysts. In the case of the Lewis acid sites, a decrease in their number is also observed with the increase in the temperature (Table S2). However, these reductions seem to be much smaller for the parent and steamed HY zeolites than for the other dealuminated zeolites (Table 1), revealing that the LAS on the former have stronger acidity strength. This clearly shows that the additional EFAl species introduced by the dealumination treatments did not lead to very strong LAS. Indeed, this may be a result of the high Si/Al ratio of the zeolite sample which normally results in EFAl with weak or no strong LAS species after dealumination [47]. Due to this, the higher the number of additional LAS on the dealuminated zeolites, the lower the ratio of LAS at 350 and 150 ℃, as it can be seen in Table 1. Similarly, with the increase in temperature, a decrease in the number of LAS is observed for all the Ni-loaded samples. As a result, it mainly appears that all the zeolites after Ni incorporation have roughly the same number of strong LAS capable of retaining pyridine at 350 °C. Therefore, it may be inferred that most of additional Lewis acidity produced by the metal appears to be rather weak in nature.

3.2.4. *Additional characterisation on Ni-impregnated zeolite samples*

Fig. 5a shows the TEM images of the various Ni-impregnated dealuminated HY zeolite samples. The TEM images of the Ni-loaded HY zeolite (Ni-HY) and Ni-incorporated steamed HY zeolite (Ni-DAHY-S) were reported in a previous publication [2]. Reduced Ni incorporated HY zeolite sample showed a combination of relatively scattered larger particles on the surface with some smaller metallic Ni^0 particles. The presence of relatively larger Ni particles on the surface could explain the higher reduction in surface area of the zeolite (Table 1). The average Ni particle size for 5 % Ni on the HY zeolite was estimated to be 26 nm. Interestingly, all the Ni-loaded dealuminated HY zeolites showed more uniform and much smaller Ni particle sizes than their parent material. This could be due to the relative increase in the textural properties of the zeolite samples after dealumination that may have allowed the migration of the Ni particles (i.e., ionic radius of Ni species is 0.69 Å [48]) to deeper positions of the zeolite framework (i.e., supercage (13 Å) and sodalite cage (7.4 Å)), as later discussed in H_2-TPR. However, it is necessary to note that the TEM analysis performed in this work only allows the analysis of the distribution of the particles located closer to the external surface of the zeolite, with little visualization of the particles confined in the pores. In detail, DAHY-HCl with maximum degree of dealumination and external surface area showed the smallest average Ni particle size (7 nm), whereas DAHY-CO_2 with the least porosity and external surface area (Table 1) showed larger Ni particle size distribution (11 nm). On the other hand, both Ni-DAHY-S and Ni-DAHY-CS with relatively similar external surface area showed average Ni particle sizes of 9 and 8 nm, respectively. The observed uniform distribution of Ni with smaller particle sizes over the dealuminated HY zeolites may be ascribed to the removal of FAl and/or EFAl from the structure, which possibly changed the electronic charge distribution on the surface of HY and affected the Ni dispersion.

Fig. 5b shows the DRS UV-Vis spectra of the bulk NiO and various Ni-loaded zeolite samples after calcination. The pure NiO showed prominent bands at around 235, 350, 420, 640, and 720 nm. Comparing to the bands associated with NiO, all Ni-loaded zeolite samples showed one broad band at around ~250–300 nm, which represented the presence of NiO species in these samples. Interestingly, a small band around ~410 nm can also be seen in the magnification insert in Fig. 5b, which shows the presence of some octahedrally coordinated Ni^{2+} particles in exchange positions [46]. However, the dominant Ni specie on all the samples is NiO.

Moreover, Fig. 5c demonstrates the H_2-TPR profiles of Ni-loaded parent and dealuminated HY zeolite samples. H_2-TPR was used to estimate the actual amount of Ni (wt%), its reducibility and infer on the location of the Ni species present in the zeolite samples. According to the literature, peaks below 400 ℃ are typical of NiO species on the outer

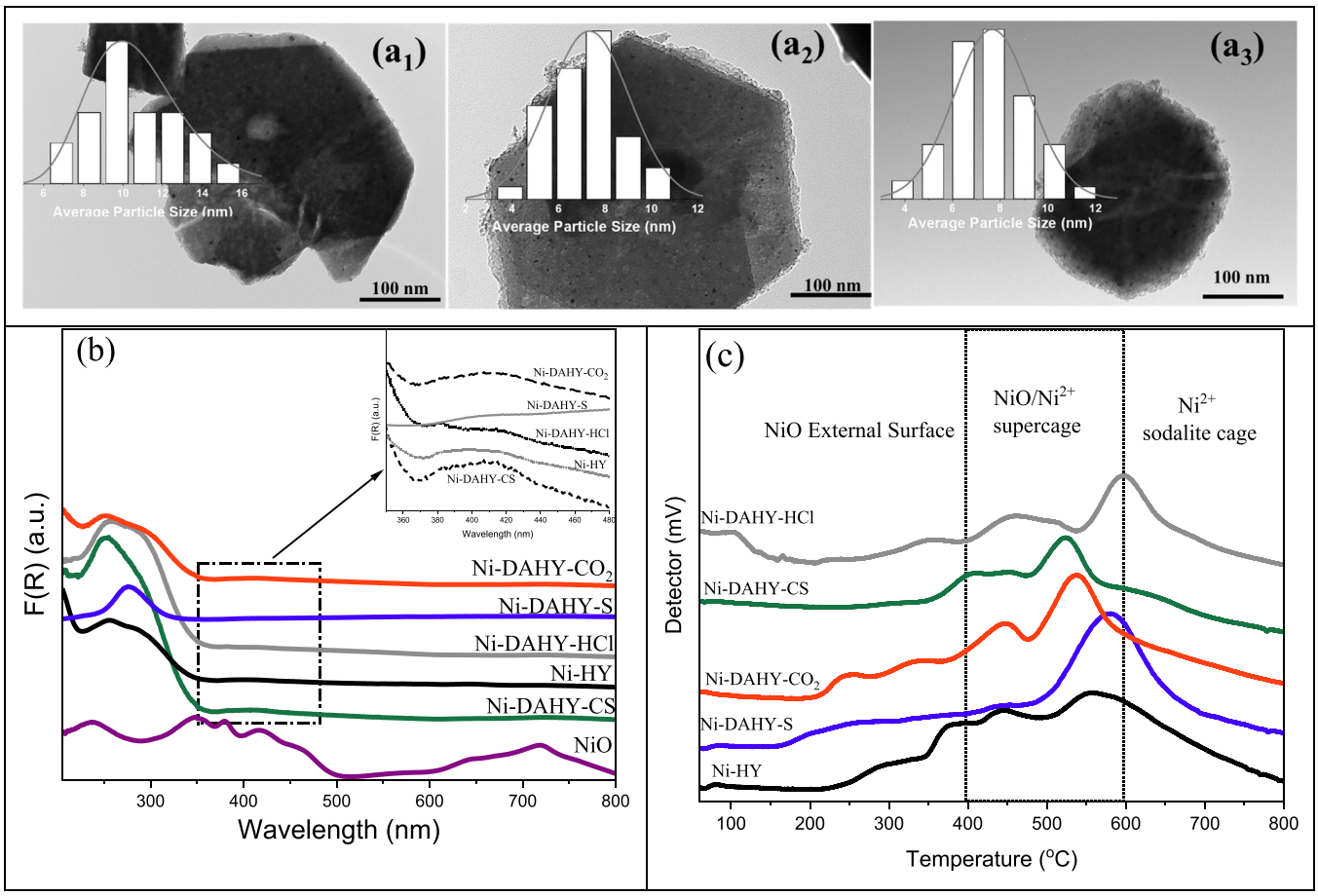

Fig. 5. TEM micrographs with Ni particle size distribution for (a_1) Ni-DAHY-CO_2 (a_2) Ni-DAHY-HCl and (a_3) Ni-DAHY-CS, (b) DRS-UV-Vis spectra and (c) H_2-TPR profiles of different Ni-loaded HY zeolite samples.

surface with weak interaction with the zeolite. Similarly, peaks between 400 and 600 ℃ are associated with NiO and/or Ni^{2+} species at the supercages with strong interaction, and peaks above 600 ℃ are associated with Ni^{2+} species at the sodalite cages with strong interaction with the support [46]. Based on the calculations, the actual amount of Ni (wt %) over the different Ni-loaded samples is as shown in Table 1. All the Ni-loaded samples showed a small variation in the actual loading of Ni (4–5 wt%). The decrease in the real amount of Ni might be due to some losses during the impregnation process. In fact, this is quite common as already seen in the literature [46,49]. Moreover, in terms of location of the Ni species present in the zeolite samples, Ni-HY showed three main distinct peaks with almost similar intensities at 375 ℃, 460 ℃ and 560 ℃. The existence of these peaks suggests the presence of uniformly distributed NiO and NiO/Ni^{2+} species on the external surface and supercages of the zeolite, respectively. On the opposite, all Ni-loaded dealuminated samples showed their most intense peaks mainly between 400 and 600 ℃, suggesting the presence of NiO/Ni^{2+} mostly within the supercages. Therefore, the increase in the textural properties for the dealuminated zeolite samples when compared to the parent HY zeolite could be at the origin of the observed behaviour, as it would allow the migration of the Ni species to deeper locations of the zeolite framework, most likely leading to smaller particle size distribution as already discussed in TEM. In detail, both Ni-DAHY-CO_2 and Ni-DAHY-CS samples presented two distinct peaks, one around 450 ℃ and another major peak around 540 ℃. For the Ni-DAHY-S Ni-DAHY-HCl catalysts, peaks appear at 441℃ and 579 ℃ and 480 ℃ and 600 ℃, respectively. This means that their most intense peaks with maxima at around 600 ℃ are displaced to higher temperatures when compared to the other two dealuminated zeolites. Thus, this observation could indicate a stronger interaction of the Ni particles with the zeolite support or the existence of metal also on the sodalite cages, in the case of the Ni-DAHY-S and Ni-DAHY-HCl. A stronger interaction of the Ni particles could only be understood if particles were significantly smaller, which is not the case. According to the TEM data, the size of the metal particles for all dealuminated zeolites is similar. However, the DAHY-S and DAHY-HCl zeolites present a higher mesoporous volume and external surface area, which may have contributed to a deeper migration of the Ni particles possibly reaching positions closer to the sodalite cages.

4. Hydrocracking experiments

4.1. Catalytic activity and selectivity

Fig. 6a shows the results obtained from the hydrocracking of virgin HDPE at 325 ℃, 20 bar initial cold H_2 pressure for 1h of reaction time. Under non-catalytic conditions, virtually no cracking was observed (~1 % conversion). However, the addition of the parent HY zeolite notably improved the conversion of HDPE to 39.3 %. This demonstrates the benefits of utilizing a catalyst for the hydrocracking of HDPE, as already observed in a previous paper [2]. Despite having significant porosity, the parent HY zeolite demonstrated significant diffusional limitations, leading to an undesirable high selectivity of heavier oils (36.5 %). This highlighted the need to investigate various dealuminated HY zeolites with better textural properties (i.e., less diffusional limitations) for the hydrocracking of HDPE.

In comparison to parent HY, all dealuminated HY zeolite samples showed enhanced conversions (Fig. 6a). Overall, an increase in the activity of the samples is observed in the following order: HY < DAHY-S <

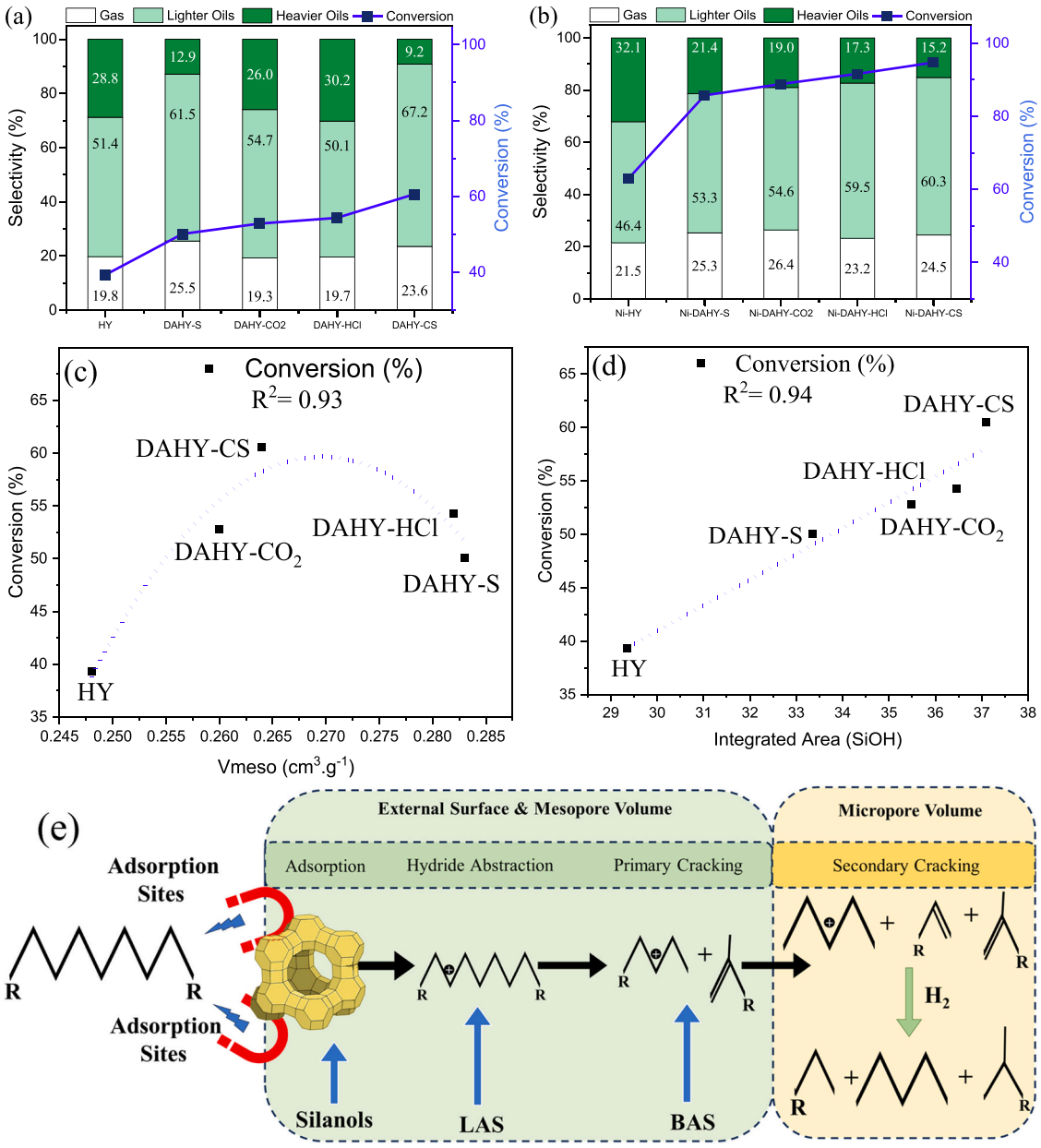

Fig. 6. (a,b) Performance comparison and product distribution of catalytic hydrocracking of virgin HDPE using different catalysts in a 300 mL autoclave reactor, 20 bar initial cold H_2 pressure, feed to catalyst ratio of 20:1 (by weight), 325 ℃ for 1h reaction time, (c) Relationship between conversion and mesopore volume of various zeolite samples (d) Relationship between conversion and terminal silanols, and (e) Reaction scheme for the hydrocracking of a straight chain paraffin over a monofunctional zeolites.

DAHY-CO_2 < DAHY-HCl < DAHY-CS. This could be thought to be primarily associated with their improved textural properties, mainly mesoporous volume and external surface area. Indeed, the enhanced external surface area of the dealuminated HY zeolite samples may help the surface cracking of the large polymeric chains into medium and shorter chains. These medium and shorter chain molecules will then more easily diffuse within the zeolite framework owing to the enhanced mesoporosity, being able to interact with a higher number of active acid sites and leading to the rapid production of lower chain hydrocarbons. Although this is true when comparing the HY zeolite with the dealuminated samples, interestingly the relationship between conversion and mesopore volume amongst the various dealuminated zeolites does not follow a linear trend (Fig. 6c). This suggests that the conversion is influenced by other factors (i.e., acidity) beyond textural properties.

To further explore other factors affecting conversion, Fig. 6e describes the mechanism for the hydrocracking of a straight chain polymer. In general, over a monofunctional zeolite, the reaction starts with the adsorption of the molten polymer on the external surface of zeolite. The presence of terminal silanols is claimed to favour the interaction between the plastic molecules and the catalytic sites [35]. In detail, terminal silanol groups appear to provide additional adsorption sites on the zeolite surface where the molten polymer can interact with the catalyst, primarily helping in the initiation of the hydrocracking of plastics by the acidic sites. Therefore, soon after the adsorption of molten polymer on the external surface of zeolite, the cracking mechanism starts over the external surface of zeolite via the classical β-scission mechanism [50]. The first step involves the formation of a carbenium ion either by hydride abstraction on Lewis acid sites (LAS) and/or direct proton donation on the Brønsted acid sites (BAS). However, based on the previous literature, LAS of the zeolite were found to be more relevant in comparison to BAS for the initiation of the hydrocracking of plastics [51]. Therefore, zeolites with relatively higher LAS could quickly form

carbenium ions, which would be followed by isomerization and cracking (β-scission) on the Brønsted acidic sites to produce medium carbenium ions and olefins [52]. The as-formed medium chain intermediates would be able to diffuse into the pores for secondary cracking. Thus, while LAS have more impact on the initiation of the cracking mechanism, zeolites with high BAS promote further the cracking of medium-chain hydrocarbons into short ones. Finally, the presence of hydrogen (P_{H2}) leads to the hydrogenation of the olefins prior to their appearance in the end product. Indeed, the observed conversion trend shows a linear relationship with the number of terminal silanols (Fig. 6d). This is in accordance with the previous studies where Chen et al. [53] discussed the importance of silanol groups in the improvement of the cracking of plastics and associated them with the surface acidity of the material. Similarly, Giglio et al., [54] discussed the debromination and cracking of plastics, which was significantly enhanced by the utilization of zeolites with notable presence of terminal silanols. Therefore, besides mesoporosity and external surface area, total acidity, BAS/LAS ratio and number of silanol groups on the zeolite can also play a role in interpreting the hydrocracking of plastics.

Based on this, and despite having the maximum textural properties and relatively high total acidity (Table 1), DAHY-S showed the lowest conversion (50.1 %) amongst the dealuminated HY zeolite samples, as it presents the lowest LAS/BAS ratio (0.15) and the lowest number of silanol groups. On the other hand, DAHY-CS presents the maximum conversion (60.5 %) possibly owing to its highest number of terminal silanols and total number of acid sites amongst all the other samples (i.e., both LAS and BAS, Table 1), while having reasonable values for the textural parameters and LAS/BAS ratio (0.21). Intermediate conversion values of 52.8 and 54.3 % were obtained for DAHY-CO_2 and DAHY-HCl respectively, possibly because they have smaller total acidity (Table 1), but higher LAS/BAS ratio (0.43 and 0.28 respectively) than the other dealuminated samples, as well as intermediate number of silanol groups. The conversion for DAHY-HCl is slightly higher than for DAHY-CO_2 most likely because of the higher mesoporous volume, external surface area and number of silanol groups of the former.

Therefore, a possible ranking for the parameters influencing the activity amongst the dealuminated zeolites could also be established: silanols > total acidity > LAS/BAS ratio > textural properties.

Furthermore, all dealuminated samples showed better selectivity towards lighter oils than the parent HY zeolite. This is not strange considering that retention time of molecules was decreased owing to the opening of the pores, which prevents secondary cracking. However, in comparison to DAHY-S and DAHY-CS, both DAHY-CO_2 and DAHY-HCl showed higher selectivity of heavier oils (26–30 %) with a consequent lower selectivity for lighter oils and gases. This increase in the selectivity of heavier oils could be attributed to the lower total acidity, and especially the Brønsted acidity, of the DAHY-CO_2 and DAHY-HCl samples, which leads to a decrease in the preponderance of the secondary cracking of heavier oils into lighter ones, as discussed in the reaction mechanism [55]. Similar results were reported by Aguado et al., [56] who studied the hydrocracking of LDPE over a hierarchical Beta zeolite. The enhanced textural properties of the hierarchical Beta zeolite promoted the catalytic cracking of LDPE as compared to the parent Beta, however the decrease in acidity led to a product shift from lower hydrocarbons to higher hydrocarbons.

Moreover, the addition of a metallic source (Ni) to the parent and dealuminated HY zeolite samples was investigated to analyze the role of bifunctional metal-acid catalysts on the cracking of HDPE (Fig. 6b). Compared to the parent HY zeolite, Ni-modified HY exhibits improved conversion. Overall, the incorporation of 5 wt% Ni to the HY zeolite increased the conversion to 62.9 %. This increase in the conversion in the presence of Ni is due to the increase in the number of Lewis acid sites (Table 1), which can have a double role in the initiation of the β-scission cracking mechanism. They can promote hydride abstraction directly forming the first carbenium ions and/or the formation of alkenes by dehydrogenation, which can subsequently be protonated on the Brønsted acid sites and form the carbenium ions [2]. The addition of Ni, however, slightly decreased the selectivity of lighter oils (46.4 %) with an increase in the affinity of heavier oils (32.1 %). The observed decrease may be associated with a decrease in the concentration of Brønsted acidity. A similar trend has been previously observed by Costa et al., [46] who studied the hydrocracking of HDPE over a USY. The addition of Ni over the USY zeolite resulted in an increase in the selectivity of heavier hydrocarbons due to a significant reduction in BAS.

Additionally, the incorporation of 5 wt% of Ni into the various dealuminated HY zeolite samples led to a remarkable increase in the conversion (Fig. 6b) This can be attributed to the combined effect of improved diffusion rates, increased number of silanol groups and more uniform distribution of Ni, with smaller average particle sizes, compared to the Ni-HY. Interestingly, despite the changes in the total acidity and LAS/BAS ratio in the Ni-dealuminated samples as compared to their fresh counterparts, conversion trends remained the same as those previously reported for the zeolites without Ni. This may corroborate that number of silanol groups is indeed a major factor affecting activity, as these were not significantly changed by Ni addition (Table 1). Despite the higher conversions achieved with the Ni-dealuminated zeolites, generically the product selectivity remained identical, in comparison to their monofunctional counterparts (Fig. 6b). Only a slight decrease in the selectivity of lighter oils was observed after the addition of Ni. For Ni-DAHY-S and Ni-DAHY-CS, this decrease was accompanied by an increase in heavier oils when compared to the samples without Ni and may be due to the significant reduction in the Brønsted acid sites. On the other hand, the same was not observed for Ni-DAHY-CO_2 and Ni-DAHY-HCl, for which an increase in the selectivity of gases was noticed instead. While a reduction in the Brønsted acidity also took place for these samples after Ni addition, this was not as pronounced as for the Ni-DAHY-S and Ni-DAHY-CS, which together with the higher activity of the Ni-impregnated zeolites could have resulted in an increase in the gas fraction.

Further analysis on the differences between the catalytic activity of various Ni-loaded zeolite samples is discussed in SI information when analysing the effect of the temperature (Table S3 and Fig. S3).

4.2. Liquid products distribution

A more detailed analysis of the *n*-heptane soluble liquids (i.e., lighter oils) was also performed, as shown in Fig. 7. Based on these results, it is possible to see that HY showed low selectivity for gasoline (20.2 %) and diesel range hydrocarbons (18.7 %), with a higher selectivity of C_{19}^{+} products (61.1 %). The lower selectivity of middle distillates (C_5-C_{18}= 38.9 %) could be due to the fact that products obtained after the initial cracking reactions were not able to completely migrate to the interior of the framework to undergo further cracking in the micropores of the zeolite. In addition, compared to parent HY zeolite, all the dealuminated HY zeolite samples showed higher selectivity for middle distillates. This shows the importance of the improved textural and acidic properties of the dealuminated HY zeolites for the cracking reactions. As expected, DAHY-CS with maximum activity and highest total acidity, especially BAS (Table 1), showed the highest selectivity for middle distillates (74.5 %). On the other hand, DAHY-CO_2 and DAHY-HCl with relatively lower BAS (Table 1) showed lower selectivity of middle distillates (46–50 %).

Furthermore, compared to the parent HY zeolite, Ni-loaded HY showed higher selectivity towards middle distillates (C_5-C_{18}= 56.1 %), with the depletion of higher hydrocarbons (C_{19}^{+} = 43.9 %), due to the additional Lewis acid sites that increase the cracking ability of the catalyst (Fig. 7b). All Ni-loaded dealuminated HY zeolite samples showed even more remarkable selectivity towards middle distillates production, especially gasoline range fuels (C_5-C_{12}), with little affinity towards higher hydrocarbons. Overall, the improved selectivity for gasoline range products over the Ni-loaded dealuminated HY zeolites might be attributed to their enhanced porosity, which leads to a more

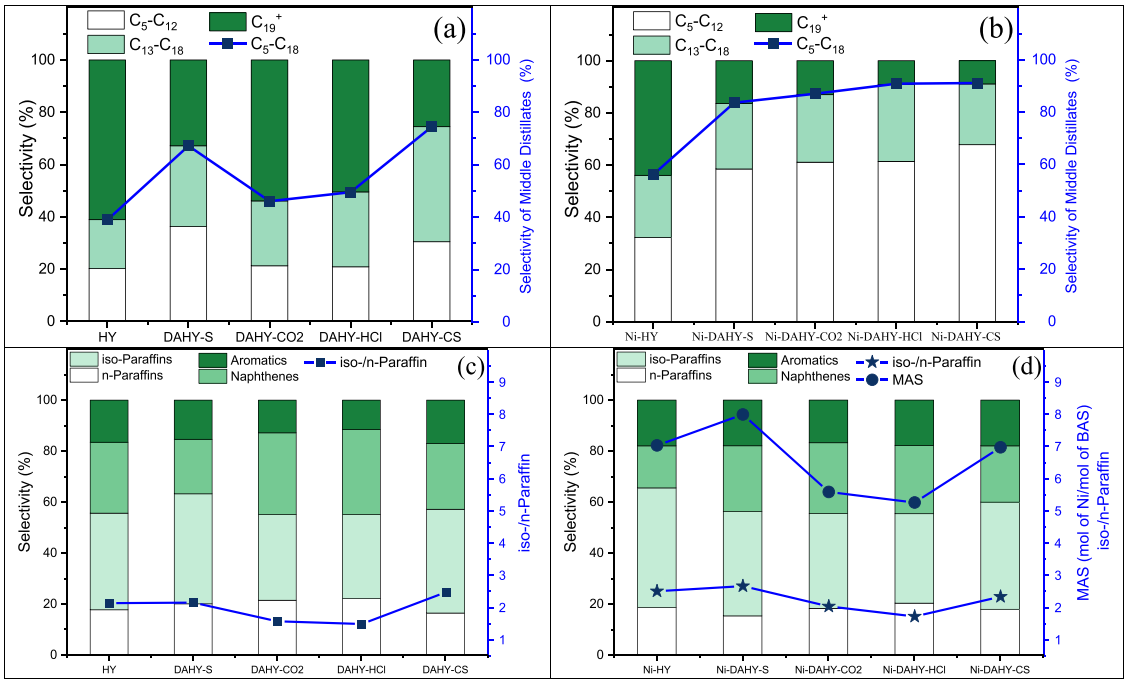

Fig. 7. Selectivity of the *n*-heptane soluble liquids obtained by the hydrocracking of virgin HDPE in a 300 mL autoclave reactor, 20 bar initial cold H_2 pressure, feed to catalyst ratio of 20:1 (by weight), 325 ℃ for 1h reaction time: (a,b) product selectivity based on carbon number and (c,d) product selectivity of paraffins, naphthenes and aromatic within gasoline range hydrocarbons over parent and modified HY zeolite samples.

even distribution of the Ni particles with a smaller average size (as confirmed by TEM), favouring the cracking. Changes in the middle distillate production within the Ni-dealuminated samples are due to modifications in the concentration of BAS (Table 1). In fact, the higher concentration of BAS over Ni-DAHY-HCl and Ni-DAHY-CO_2 justifies the increase in selectivity of middle distillates.

Fig. 7c illustrates the product composition of parent and its modified dealuminated HY zeolite samples in the gasoline range hydrocarbons. Overall, paraffins are the dominant reaction products in the presence of HY zeolite. Additionally, HY shows higher selectivity for *iso*-paraffins (37.9 %) relatively to the *n*-paraffins (17.7 %). The higher selectivity for *iso*-paraffins over *n*-paraffins is attributed to the acid sites of the HY which play an important role in promoting the isomerization reactions that usually take place prior to the β-scission (or catalytic) cracking. Additionally, HY can favour cyclization and aromatization reactions, contributing also to the production of naphthenes (selectivity = 27.8 %) and aromatics (selectivity = 16.5 %). Compared to the parent HY zeolite, all dealuminated HY zeolite samples showed higher selectivity for paraffins. The higher selectivity for paraffins could be related to the decrease in the retention time of the molecules within the structure of the dealuminated zeolites owing to the opening of the pores, leading to a smaller occurrence of secondary transformations, such as cyclization and aromatization that conduct to the formation of naphthenes and aromatics. However, both DAHY-S and DAHY-CS showed an increase in the *iso-/n*-paraffins ratio, whereas a decrease was observed over both DAHY-CO_2 and DAHY-HCl (Fig. 7c). This could be associated with the lower BAS in DAHY-CO_2 and DAHY-HCl samples (Table 1), which could have led to a reduction in the significance of the isomerization reactions. Similarly, a decrease in BAS over DAHY-CO_2 and DAHY-HCl resulted in lower selectivity of aromatics (11–13 %), whereas both DAHY-S and DAHY-CS present slightly higher selectivity for aromatics (15–17 %).

Furthermore, addition of Ni over the HY zeolites significantly changed the product distribution, with catalysts with higher metal-acid-sites (i.e., MAS, mol Ni/mol BAS) showing higher *iso-/n*-paraffins (Fig. 7d). In general, hydrocracking over a high MAS zeolite catalyst increases the rate of isomerization on the Ni-sites, whereas a decrease in Brønsted acidity leads to a decrease in the rate of β-scission cracking, resulting in high *iso-/n*-paraffins [55]. Therefore, Ni-DAHY-S with the maximum MAS (8) showed the highest *iso-/n*-paraffin ratio of 2.7, whereas Ni-DAHY-HCl (i.e., minimum MAS value of 5.3) led to the lowest *iso-/n*-paraffin ratio (1.7 %). The maximum MAS value over Ni-DAHY-S also confirms its lower selectivity towards middle distillates as a high MAS decreases the rate of β-scission cracking over the Brønsted acid sites [32]. In addition, a slight increase in the selectivity of aromatics was observed at the expense of naphthenes. The relative increase in aromatics selectivity is due to the hydrogenation ability of Ni which promotes the formation of C-C bonds required for the production of cyclic hydrocarbons. In addition, it helps in the oligomerization and alkylation of paraffins, as wells as aromatization, which increases the selectivity for aromatics [57].

To summarize, the textural properties of various dealuminated zeolites have facilitated higher conversion of HDPE. However, the activity of the zeolites is also affected by other parameters, namely amount of silanol groups, total acidity and Lewis/Brønsted acid site ratio. Furthermore, while Lewis acidity plays a significant role in enhancing conversion, Brønsted acidity significantly contributed to the high selectivity of gasoline-range hydrocarbons with high affinity of *iso-/n*-paraffins. On the other hand, the incorporation of Ni led to a marked increase in catalytic activity, underscoring the significance of bi-functional dealuminated zeolites for the effective hydrocracking of HDPE. In general, Ni-loaded zeolites with better metal-acid-sites (MAS) demonstrated a high *iso-/n*-paraffin ratio, whereas the selectivity towards gasoline range hydrocarbons was predominantly influenced by the Brønsted acidity.

4.3. *Process optimization and reusability tests*

Hydrocracking experiments were performed at different reaction temperatures to optimize the reaction to achieve higher selectivity of gasoline range products. Similarly, to evaluate the performance of the Ni-dealuminated HY zeolites under more realistic conditions, hydrocracking experiments of actual waste HDPE (i.e., post-consumed HDPE milk bottles) were carried out under optimized reaction conditions (i.e., 375 ℃, 30 bar H_2 pressure for 45 min). The reaction conditions were

selected to achieve relatively high conversion rates (~100 %) during the fresh runs in order to minimize the impact of unburnt plastics during reusability tests. The TGA analyses of virgin and post-consumed HDPE are shown in Fig. S5. The hydrocracking results revealed almost similar performance for all Ni-loaded dealuminated HY zeolites with waste HDPE, indicating the equal effectiveness of all Ni-dealuminated HY zeolites in breaking down the polymeric chains of HDPE to fuels. These results are presented in SI (Table S5 and Fig. S6).

Furthermore, the reusability and stability of these Ni-dealuminated HY zeolites for the hydrocracking of post-consumed HDPE at optimized reaction conditions were evaluated. In catalyzed reactions, it is important to assess the stability of catalysts from economic and technological considerations. Therefore, all Ni-loaded dealuminated HY zeolites were used in consecutive reaction runs to determine whether they can be used without the need to be regenerated. The catalysts were recovered, washed, and completely dried after each run so that they could be used in the subsequent run. Following the 3rd cyclic run (i.e., Spent II), the recovered catalysts were subjected to a regeneration process involving calcination at 500 ℃ under air flow followed by reduction at 500 ℃ under H_2. All experiments were performed under the same reaction conditions.

Table 2 shows the results for the different Ni-loaded dealuminated HY zeolites for the hydrocracking of post-consumed HDPE in consecutive reaction runs over fresh, spent and regenerated catalysts. Overall, all the catalysts showed to be relatively stable when submitted to consecutive reaction runs. However, while the conversion remained practically unaltered over the two first cyclic runs, a more noticeable decline in catalyst activity was observed between the 2nd and the 3rd reaction runs. Here, Ni-DAHY-CO_2 showed the lowest stability in the 3rd run, while Ni-DAHY-CS revealed to be the best-performing catalyst in consecutive runs. The maximum decrease in the activity for Ni-DAHY-CO_2 was due to the combined effect of significant decrease in the sample porosity as a result of coke deposition and Ni particles sintering (vide infra). In addition, all the catalysts only showed a small change in the catalytic selectivity for gases and liquids. Overall, the selectivity for gases and lighter oils decreased, whereas the selectivity for heavier oils increased with the number of runs. This is not strange considering that the catalysts are losing their ability to perform cracking. To determine the reasons for the observed behaviours of the used Ni-loaded dealuminated HY zeolites, the spent catalysts after the first, second and/or third reaction runs were studied by TGA (Fig. S7 and Table S6), XRD (Fig. S8), TEM (Fig. S9), and nitrogen physisorption (Table S7). The detailed discussion is part of the SI information. Briefly, the combination of partial obstruction of the porosity by coke deposition and Ni particles sintering appear to be responsible for the decrease in external surface area and possibly deactivation of the catalysts during the cycles. The Ni-DAHY-CO_2 appears to be overall the most affected, in agreement with the highest activity decay observed in the third consecutive reaction run.

Table 2
Performance comparison and product distribution for the hydrocracking of HDPE over fresh, spent and regenerated spent catalysts.

Catalyst	Material	Yield (%) (Selectivity (%))			Conv. (%)
		Gases	Lighter Oils	Heavier Oils	
Ni-DAHY-S	Fresh Run	26.6 (26.9)	64.9 (65.6)	7.4 (7.5)	98.9
	Spent I	24.6 (26.5)	58.2 (62.8)	10.0 (10.8)	92.8
	Spent II	23.9 (27.2)	48.6 (55.2)	15.4 (17.5)	87.9
	Regenerated Run	23.4 (24.6)	60.8 (64.1)	10.7 (11.2)	94.8
Ni-DAHY-CO_2	Fresh Run	28.7 (28.9)	63.7 (64.4)	6.9 (7.0)	>99
	Spent I	24.4 (25.6)	62.7 (65.7)	8.3 (8.7)	95.4
	Spent II	21.4 (25.2)	47.5 (55.9)	16.0 (18.8)	84.8
	Regenerated Run	21.2 (22.1)	61.6 (64.4)	12.8 (13.4)	95.6
Ni-DAHY-HCl	Fresh Run	30.3 (30.5)	62.9 (63.3)	6.2 (6.3)	>99
	Spent I	26.1 (27.2)	62.7 (65.3)	7.2 (7.5)	95.9
	Spent II	23.6 (26.2)	55.8 (61.8)	10.8 (12.0)	90.2
	Regenerated Run	30.2 (31.2)	58.9 (60.9)	7.6 (7.9)	96.7
Ni-DAHY-CS	Fresh Run	33.4 (33.6)	60.2 (60.5)	6.0 (6.0)	>99
	Spent I	23.3 (24.0)	64.0 (65.8)	9.9 (10.2)	97.2
	Spent II	21.9 (23.7)	58.5 (63.2)	12.2 (13.2)	92.7
	Regenerated Run	31.9 (32.6)	59.1 (60.4)	6.8 (7.0)	97.8

Reaction conditions: 30 bar initial cold H_2 pressure, post-consumed HDPE to catalyst ratio of 20:1 (by weight) for 45 min reaction time at 375 ℃.

Moreover, all the spent catalysts after the 3rd cyclic run were regenerated and reused for the hydrocracking of post-consumed HDPE. All the catalysts showed a significant increase in the overall conversion as compared to the third run, with values approaching the ones obtained in the second reaction run. The overall increase in the conversion over the regenerated catalysts is due to the enhanced textural properties of the catalysts after being calcined and reduced, as shown in Table S7. Additionally, there is a possibility that the Ni metal particles underwent redistribution as a consequence of the thermal treatment, as confirmed by the TEM analysis (Fig. S10). In general, the results indicate a little decline in the catalytic performance for all the Ni-dealuminated HY zeolites following cyclic runs. However, they are able to recover their catalytic activity after an efficient regeneration process.

Fig. 8 demonstrates the comparison of product selectivity for *n*-heptane soluble oils obtained from the hydrocracking experiments over fresh, spent and regenerated Ni-loaded dealuminated HY zeolite samples. Each catalyst showed a similar trend with the overall difference being in the selectivity for gasoline range hydrocarbons in each cyclic run. Indeed, the product selectivity shifted from gasoline (i.e., C_5-C_{12}) to higher hydrocarbon range fuels with the increase in the number of reaction cycles. This is because of the obstruction of active sites by coke and increase in the Ni particles size, which resulted in a decreased cracking ability of the catalyst. As expected, the Ni-DAHY-CO_2 showed a more pronounced decrease in the selectivity for gasoline from 85.6 % to 48.5 % and a significant increase of C_{13}^{+} fuels from 14.4 % to 51.5 %, as a result of its higher activity loss. After regeneration, all Ni-loaded dealuminated Y zeolite samples exhibited again a higher cracking ability, which resulted in an increased selectivity for gasoline range fuels as shown in Fig. 8. The increased selectivity to gasoline range hydrocarbons for all regenerated catalysts is due to the elimination of certain carbonaceous materials by calcination and the redistribution of the Ni particles with the thermal treatment, as previously explained.

In addition, all the spent catalysts showed an increase in the selectivity for *n*-paraffins and aromatics at the expense of naphthenes and *iso*-paraffins when submitted to the consecutive runs (Fig. 8). This could be due to the partial deactivation of Ni-loaded dealuminated zeolites over successive cycles because of coke deposition on active (acidic) sites which resulted in overall poor cracking, as well as isomerization of *n*-paraffins to *iso*-paraffins and cyclization to naphthenes. In addition, with the structure being partially obstructed, the diffusion of the *iso*-paraffins (bulkier than *n*-paraffins) to the exterior of the structure becomes more hindered. On the other hand, the dehydrogenation capability of the catalysts on the Ni Lewis acid sites does not appear to have been compromised in great extent by the carbonaceous materials accumulation neither by the increase in particles size, which explains the decrease in the naphthenes to aromatics ratio with the number of reaction cycles.

After regeneration, an opposite trend is observed, as all the Ni-loaded dealuminated zeolites showed an increase in the selectivity for *iso*-paraffins and naphthenes with a decrease in the selectivity for *n*-paraffins. This boost in the selectivity is obviously due to removal of the carbonaceous materials with a consequent enhancement in the textural properties and access to the active sites, as previously explained. Therefore, the obtained results suggested that all the Ni-loaded dealuminated HY zeolites could be regenerated to achieve similar activity and comparable product selectivities to that of fresh catalysts, showing potential feasibility for industrial applications.

To conclude, the state-of-the-art modified dealuminated zeolites

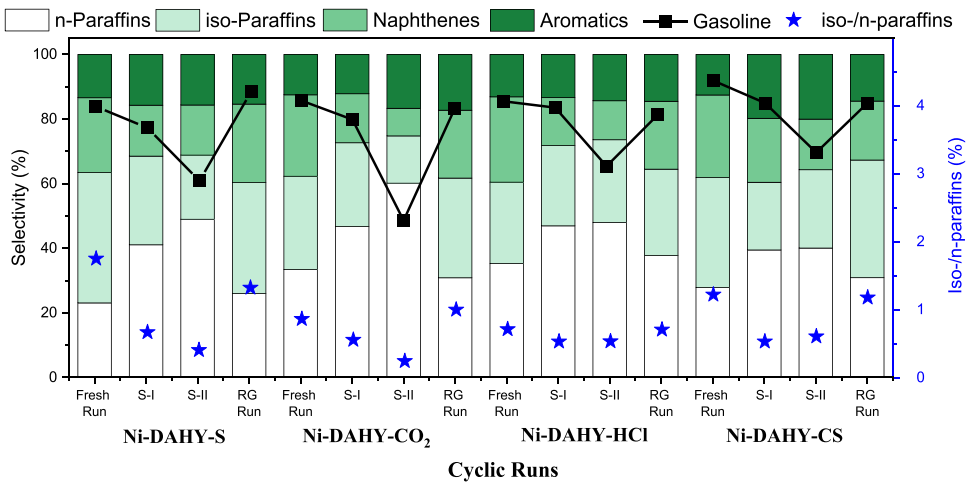

Fig. 8. Selectivity of the *n*-heptane soluble liquids obtained by the hydrocracking of post-consumed HDPE over fresh, spent (S-I and S-II) and regenerated (RG) spent catalysts in a 300 mL autoclave reactor, at 375 ℃ under 30 bar initial cold H_2 pressure, feed to catalyst ratio 20:1 for 45 min. Upper line represents the selectivity of gasoline range hydrocarbons whereas bars shows the selectivity of product composition in the same range. Lower points illustrate the trend in *iso-/n*-paraffin ratio during the reusability tests.

showed comparable or even better catalytic activity and selectivity for gasoline range fuels to that of traditionally modified dealuminated samples obtained through harsh temperature and acid treatments. Similarly, the novel synthesized Ni loaded dealuminated zeolites showed comparable stability and activity after regeneration. Therefore, the as-proposed convective steamed and molecular CO_2 assisted modified dealuminated zeolites highlight the potential for advanced innovative technologies in the production of dealuminated zeolites with exceptional activity and less environmental impacts, but also with industrial relevance. Under the context of this study, the forced convective steamed dealuminated zeolite revealed to be more appealing, since this method was not only effective in modifying the structure of the zeolite in lesser time and with lower impact on the environment than the other dealumination routes, but it also led to the best catalytic results in terms of HDPE conversion, selectivity for lighter oils and stability.

The performance of the various Ni-loaded hierarchical zeolites for the hydrocracking of post-consumed HDPE was also compared with the recent studies for the hydrocracking of PE (Table S8). Based on the literature comparison, different acid catalytic supports with and without the addition of metal were utilized for the hydrocracking of polyethylene to produce value-added chemicals (i.e., gases and/or liquids). However, most of the synthesis and modification techniques rely on the use of complex, energy extensive, costly, time consuming and environmentally unfriendly procedures, which violate the green chemistry metrics and sustainable practices. Similarly, in terms of product distribution, the catalysts showed good activity. However, they produce a wide range of liquid products or require much longer reaction time to produce narrow range lower hydrocarbons. On the opposite, the proposed greener and more sustainable Ni-loaded dealuminated zeolites showed better activity and selectivity, in the gasoline range fuels.

5. Conclusion

The present study highlights novel methods, via forced convective steaming and use of molecular CO_2, to mildly and more sustainably dealuminate HY zeolite, achieving enhanced porosity and external surface area, with comparable acidic properties, in less time and with lower environmental impact than their rival traditional counterparts obtained via steaming and acid leaching. Indeed, DAHY-CS showed the least impact of 0.09 kg CO_2 eq./g on global warming, whereas acid leaching through HCl generated maximum global warming potential of 3.48 kg CO_2 eq./g. A similar trend was seen where both DAHY-CS and DAHY-CO_2 showed either similar or lower impact on freshwater aquatic ecotoxicity (FWAE), in comparison to their respective traditional methods.

Moreover, all modified dealuminated HY zeolites with and without the addition of Ni were compared with the parent HY zeolite for the hydrocracking of HDPE at 325 ℃ for 1h at 20 bar cold H_2 pressure. All the dealuminated HY zeolites showed better conversion of HDPE with significantly improved selectivity for lower hydrocarbons. Amongst the different dealuminated samples, DAHY-S revealed the least cracking ability because of the relatively lower silanol groups and the least concentration of Lewis acid sites. On the other hand, DAHY-CS resulted in the maximum conversion of HDPE to gasoline range fuels, which was ascribed to the presence of maximum silanol groups, combined with high concentration of acid sites and notable porosity. The addition of Ni remarkably enhanced the conversion to >85 % for all Ni-loaded dealuminated HY zeolite samples with maximum selectivity for gasoline range fuels. Furthermore, the reusability experiments of all Ni-loaded dealuminated samples for the hydrocracking of post-consumed HDPE revealed that the activity of the catalyst is only slightly impacted by coke deposition and sintering of the Ni particles. However, all regenerated catalysts showed similar activity and comparable selectivity to those of their fresh counterparts, which was due to the removal of coke and redistribution of the Ni particles during the regeneration process.

Overall, under the context of this work, dealumination via forced convective steaming seems to be a preferable dealumination route owing to its lowest environment impact and best catalytic performance. Hence, the present study confirms the importance and applicability of the presented novel and greener routes for the dealumination of zeolites, opening the field for further optimisation of these dealumination methods and the design and development of more sustainable zeolites for environmental-related applications.

CRediT authorship contribution statement

Muhammad Usman Azam: Writing – original draft, Investigation, Conceptualization. **Waheed Afzal:** Writing – review & editing, Supervision, Resources, Conceptualization. **Auguste Fernandes:** Writing – review & editing, Investigation. **Inês Graça:** Writing – review & editing, Supervision, Resources, Conceptualization.

Declaration of Competing Interest

The authors declare the following financial interests/personal relationships which may be considered as potential competing interests:

Muhammad Usman Azam reports financial support was provided by Leverhulme Trust. Auguste Fernandes reports financial support was provided by Foundation for Science and Technology. Waheed Afzal, Muhammad Azam Usman, Inês Graça have patent #no. 2400590.2 and no. 2400596.9 pending to UK Patent Office. If there are other authors, they declare that they have no known competing financial interests or personal relationships that could have appeared to influence the work reported in this paper.

Data Availability

All data is provided either on the manuscript or as supporting information.

Acknowledgements

This study was funded by The LEVERHULME TRUST (Grant DS-2017–073). Muhammad Usman Azam, a Leverhulme Trust Doctoral Scholar, is part of the 15 PhD scholarships of the "Leverhulme Centre for Doctoral Training in Sustainable Production of Chemicals and Materials" at the University of Aberdeen (Scotland, United Kingdom). Auguste Fernandes thanks Portuguese FCT for funding (CQE - UIDB/00100/2020 and UIDP/00100/2020; IMS - LA/P/0056/2020; contract hiring under DL57/2016 law). The authors also acknowledge Dr Alan McCue (University of Aberdeen, UK) and Gillian Milne (Senior Histology Technician, UoA) for providing technical support during catalyst characterizations.

Appendix A. Supporting information

Supplementary data associated with this article can be found in the online version at doi:10.1016/j.apcata.2024.119873.

References

[1] Q. Sun, N. Wang, J. Yu, Q. Sun, J. Yu, N. Wang, (2021).
[2] M. Usman Azam, A. Fernandes, I. Graça, W. Afzal, Fuel 349 (2023) 128704.
[3] M.U. Azam, A. Vete, W. Afzal, Molecules 27 (2022) 8084, 2022, Vol. 27, Page 8084.
[4] B. Liu, W. Lu, Y. Liu, Q. Feng, Y. Huang, J. Shang, Y. Zhu, J. Dong, AIChE J. (2023) e18201.
[5] D. Yao, H. Yang, H. Chen, P.T. Williams, Appl. Catal. B 227 (2018) 477–487.
[6] N.V. Kolesnichenko, N.N. Ezhova, Y.M. Snatenkova, J. Dai, J. Wang, Z. Liu, J. Phys. Conf. Ser. 2459 (2023) 012056.
[7] C. Fernandez, I. Stan, J.P. Gilson, K. Thomas, A. Vicente, A. Bonilla, J. Pérez-Ramírez, Chem. - A Eur. J. 16 (2010) 6224–6233.
[8] J. Wang, Y. Li, M. Liu, Z. Li, X. Gao, D. Yang, Chempluschem 85 (2020) 2290–2297.
[9] M. Umer, C. Brandoni, M. Jaffar, N.J. Hewitt, P. Dunlop, K. Zhang, Y. Huang, Processes 12 (2024) 112, 2024, Vol. 12, Page 112.
[10] W.H. Hu, M.N. Liu, Q.X. Luo, J. Zhang, H. Chen, L. Xu, M. Sun, X. Ma, Q.Q. Hao, Chem. Eng. J. 466 (2023) 143098.
[11] M. Muñoz, I. Morales, C.S. Costa, M. Multigner, P. de la Presa, J.M. Alonso, J. M. Silva, M.D.R. Ribeiro, B. Torres, J. Rams, Materials 14 (2021) 1–15.
[12] A. Bin Jumah, V. Anbumuthu, A.A. Tedstone, A.A. Garforth, Ind. Eng. Chem. Res 58 (2019) 20601–20609.
[13] Y. Zhang, X. Lin, N. J. Chem. 47 (2023) 6943–6950.
[14] J. Xie, X. Li, J. Guo, L. Luo, J.J. Delgado, N. Martsinovich, J. Tang, Nat. Commun. 14 (2023) 1–12, 2023 14:1.
[15] Y. Wang, J. Yu, F. Yang, Y. Zhao, J. Zhuang, X. Lu, X. Zhu, K. Zhu, Ind. Eng. Chem. Res 62 (2023) 10012–10023.
[16] S. Wang, J. Jiang, M. Gu, F. Gao, Z. Shen, RSC Adv. 13 (2023) 734–741.
[17] L.H. Chen, M.H. Sun, Z. Wang, W. Yang, Z. Xie, B.L. Su, Chem. Rev. 120 (2020) 11194–11294.
[18] P. Peng, X.-H. Gao, Z.-F. Yan, S. Mintova, Natl. Sci. Rev. 7 (2020) 1726–1742.
[19] Z. Zhu, H. Ma, W. Liao, P. Tang, K. Yang, T. Su, W. Ren, H. Lü, Appl. Catal. B 288 (2021) 120022.
[20] S. Abdulridha, R. Zhang, S. Xu, A. Tedstone, X. Ou, J. Gong, B. Mao, M. Frogley, C. Bawn, Z. Zhou, X. Zhang, S. Chansai, S.M. Holmes, C. Hardacre, A.A. Garforth, S. Yang, Y. Jiao, X. Fan, Microporous Mesoporous Mater. 311 (2021) 110715.
[21] X. Jiao, Z. Hu, K. Zheng, J. Zhu, Y. Wu, X. Zhang, J. Hu, W. Yan, J. Zhu, Y. Sun, Y. Xie, Nano Lett. 22 (2022) 10066–10072.
[22] A. Lal, H. Chen, Appl. Catal. A Gen. 303 (2006) 9–17.
[23] R.J. Conk, S. Hanna, J.X. Shi, J. Yang, N.R. Ciccia, L. Qi, B.J. Bloomer, S. Heuvel, T. Wills, J. Su, A.T. Bell, J.F. Hartwig, Science (1979) 377 (2022) 1561–1566.
[24] G. Lopez, A. Erkiaga, M. Artetxe, M. Amutio, J. Bilbao, M. Olazar, Ind. Eng. Chem. Res 54 (2015) 9536–9544.
[25] L. Yao, J. Zhu, S. Li, Y. Ma, C. Yue, J. Therm. Anal. Calor. 147 (2022) 14257–14266.
[26] Y. Wang, L. Cheng, J. Gu, Y. Zhang, J. Wu, H. Yuan, Y. Chen, ACS Omega 7 (2022) 2752–2765.
[27] A.R. Rahimi, J.M. Garciá, Nat. Rev. Chem. 1 (2017) 1–11, 2017 1:6.
[28] F. Zhang, M. Zeng, R.D. Yappert, J. Sun, Y.H. Lee, A.M. LaPointe, B. Peters, M. M. Abu-Omar, S.L. Scott, Science (1979) 370 (2020).
[29] S. Liu, P.A. Kots, B.C. Vance, A. Danielson, D.G. Vlachos, Sci. Adv. 7 (2021) 8283–8304.
[30] R. Saab, C.M. Damaskinos, K. Polychronopoulou, A.M. Efstathiou, N. Charisiou, M. Goula, S.J. Hinder, M.A. Baker, A. Schiffer, Appl. Catal. A Gen. 630 (2022) 118437.
[31] C.S. Costa, H. Dao Thi, K.M. Van Geem, M. Rosário Ribeiro, J.M. Silva, Sustain Energy Fuels 6 (2022) 3611–3625.
[32] Z. Dong, W. Chen, K. Xu, Y. Liu, J. Wu, F. Zhang 12 (2022) 14882–14901.
[33] X. Zhou, X. Han, Z. Qu, J. Zhang, F. Zeng, Z. Tang, R. Chen, ACS Sustain Chem. Eng. (2024).
[34] M. Muñoz, I. Morales, C.S. Costa, M. Multigner, P. de la Presa, J.M. Alonso, J. M. Silva, M.D.R. Ribeiro, B. Torres, J. Rams, Materials 14 (2021) 1–15.
[35] B. Reiprich, K.A. Tarach, K. Pyra, G. Grzybek, K. Góra-Marek, ACS Appl. Mater. Interfaces 14 (2022) 6667–6679.
[36] B. Hernández, P. Kots, E. Selvam, D.G. Vlachos, M.G. Ierapetritou, (2023).
[37] V. Cappello, P. Sun, G. Zang, S. Kumar, R. Hackler, H.E. Delgado, A. Elgowainy, M. Delferro, T. Krause, (2022).
[38] O. Olafasakin, J. Ma, V. Zavala, R.C. Brown, G.W. Huber, M. Mba-Wright, Energy Fuels 37 (2023) 15832–15842.
[39] W. Lutz, Adv. Mater. Sci. Eng. 2014 (2014).
[40] L. Fan, Y. Wang, X. Zhai, Q. Yin, J. Zhang, Y. Zhu, L. Wang, Plasma Chem. Plasma Process. 43 (2023) 1979–1998.
[41] S.S. Vieira, Z.M. Magriotis, M.F. Ribeiro, I. Graça, A. Fernandes, J.M.F.M. Lopes, S. M. Coelho, N.A.V. Santos, A.A. Saczk, Microporous Mesoporous Mater. 201 (2015) 160–168.
[42] I. Graça, M.C. Bacariza, A. Fernandes, D. Chadwick, Appl. Catal. B 224 (2018) 660–670.
[43] A. Penkova, L.F. Bobadilla, F. Romero-Sarria, M.A. Centeno, J.A. Odriozola, Appl. Surf. Sci. 317 (2014) 241–251.
[44] T.H. Vuong, N. Rockstroh, U. Bentrup, J. Rabeah, J. Knossalla, S. Peitz, R. Franke, A. Brückner, ACS Catal. 11 (2021) 3541–3552.
[45] R.T.J. Gerards, A. Fernandes, I. Graça, M.F. Ribeiro, Fuel 260 (2020) 116372.
[46] C.S. Costa, M. Muñoz, M.R. Ribeiro, J.M. Silva, Sustain Energy Fuels 5 (2021) 1134–1147.
[47] Manoj Ravi, Vitaly L. Sushkevich, Jeroen A. van Bokhoven, Nat. Mater. 19 (2020) 1047–1056.
[48] S. Yousaf, S. Zulfiqar, M.N. Shahi, M.F. Warsi, N.F. Al-Khalli, M.F. Aly Aboud, I. Shakir, Ceram. Int 46 (2020) 3750–3758.
[49] L. Liao, L. Chen, R.P. Ye, X. Tang, J. Liu, Chem. Asian J. 16 (2021) 678–689.
[50] K. Pyra, K.A. Tarach, A. Śrębowata, I. Melián-Cabrera, K. Góra-Marek, Appl. Catal. B 277 (2020) 119070.
[51] K. Pyra, K.A. Tarach, A. Śrębowata, I. Melián-Cabrera, K. Góra-Marek, Appl. Catal. B 277 (2020).
[52] A. Marcilla, M.I. Beltrán, R. Navarro, Appl. Catal. B 86 (2009) 78–86.
[53] T. Chen, J. Yu, C. Ma, K. Bikane, L. Sun, Chemosphere 248 (2020) 125964.
[54] E. Giglio, A. Marino, P. Pizarro, J.M. Escola, M. Migliori, G. Giordano, D.P. Serrano, Catal. Sci. Technol. 13 (2023) 5799–5820.
[55] L. Li, H. Luo, Z. Shao, H. Zhou, J. Lu, J. Chen, C. Huang, S. Zhang, X. Liu, L. Xia, J. Li, H. Wang, Y. Sun, J. Am. Chem. Soc. 145 (2023) 1847–1854.
[56] D.P.S.J.M.R.J. Aguado, Microporous Mesoporous Mater. 115 (2008) 504–513.
[57] A. Bin Jumah, M. Malekshahian, A.A. Tedstone, A.A. Garforth, ACS Sustain Chem. Eng. 9 (2021) 16757–16769.